



UNIVERSITY OF LEEDS

This is a repository copy of *Bimolecular Reactions of Activated Species: An Analysis of Problematic HC(O)C(O) chemistry*.

White Rose Research Online URL for this paper:

<http://eprints.whiterose.ac.uk/104220/>

Version: Accepted Version

Article:

Shannon, RJ, Robertson, SH, Blitz, MA et al. (1 more author) (2016) Bimolecular Reactions of Activated Species: An Analysis of Problematic HC(O)C(O) chemistry. *Chemical Physics Letters*, 661. pp. 58-64. ISSN 0009-2614

<https://doi.org/10.1016/j.cplett.2016.08.055>

© 2016 Elsevier B.V. Licensed under the Creative Commons Attribution-NonCommercial-NoDerivatives 4.0 International
<http://creativecommons.org/licenses/by-nc-nd/4.0/>

Reuse

Unless indicated otherwise, fulltext items are protected by copyright with all rights reserved. The copyright exception in section 29 of the Copyright, Designs and Patents Act 1988 allows the making of a single copy solely for the purpose of non-commercial research or private study within the limits of fair dealing. The publisher or other rights-holder may allow further reproduction and re-use of this version - refer to the White Rose Research Online record for this item. Where records identify the publisher as the copyright holder, users can verify any specific terms of use on the publisher's website.

Takedown

If you consider content in White Rose Research Online to be in breach of UK law, please notify us by emailing eprints@whiterose.ac.uk including the URL of the record and the reason for the withdrawal request.

¹ Bimolecular Reactions of Activated Species: An ² Analysis of Problematic HC(O)C(O) chemistry

³ *Robin J Shannon¹, Struan H Robertson^{2*}, Mark A Blitz^{1,3}, Paul W Seakins^{1,3*}.*

- ⁴ 1. School of Chemistry, University of Leeds, Leeds, LS2 9JT, UK
⁵ 2. Dassault Systèmes, BIOVIA, 334 Science Park, Cambridge, CB4 0WN, UK
⁶ 3. National Centre for Atmospheric Science, University of Leeds, Leeds, LS2 9JT, UK

⁷

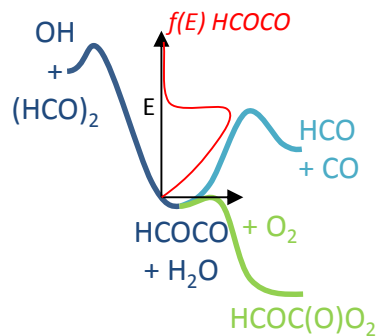
⁸ Corresponding Author

⁹ * To whom correspondence should be addressed: Struanrobertson@gmail.com,
¹⁰ P.W.Seakins@leeds.ac.uk

¹¹ ABSTRACT

¹² Experimental studies have demonstrated the importance of non-thermal bimolecular association
¹³ chemistry. Recently a fully reversible method for incorporating any number of such non-thermal
¹⁴ reactions into a single master equation has been developed (Green and Robertson, Chem Phys Lett,
¹⁵ 2014, **605**, 44-46). Using this methodology experimental results for the system: (1) $(\text{CHO})_2 + \text{OH}$
¹⁶ $\rightarrow \text{HC}(\text{O})\text{C}(\text{O}) + \text{H}_2\text{O}$, (2) $\text{HC}(\text{O})\text{C}(\text{O}) \rightarrow \text{HCO} + \text{CO}$, (3) $\text{HC}(\text{O})\text{C}(\text{O}) + \text{O}_2 \rightarrow \text{OH} + \text{CO} + \text{CO}_2$,
¹⁷ are modeled, reproducing the temperature and pressure dependence of the OH yield. An issue
¹⁸ remains as to how to model energy partition into $\text{HC}(\text{O})\text{C}(\text{O})$.

19 TOC GRAPHICS



20

21 **KEYWORDS:** Multiple reaction master equation, non-equilibrium, prior distribution, kinetics.

22

23 **Introduction**

24 One of the primary limitations in a standard master equation simulation is the inability to treat
25 multiple sequential bimolecular association processes involving activated species. The use of a
26 bimolecular source term is relatively trivial, and a number of different such terms can be readily
27 included in most master equation approaches, [1,2] however the standard bimolecular source term
28 assumes both of the bimolecular species exhibit a Boltzmann distribution of energies. Treating
29 bimolecular association reactions involving activated reaction intermediates is more challenging.
30 Recent experimental studies [3,4] have demonstrated that oxygen is capable of intercepting
31 vibrationally excited reaction intermediates with rates which are competitive with stabilization and
32 unimolecular processes under atmospheric conditions and other recent work has highlighted the
33 importance of non-Boltzmann processes in combustion chemistry [5,6]. These studies emphasize
34 the need to treat such systems using a single master equation approach.

The simplest way of treating such processes is the use of a bimolecular sink method in which the bimolecular association reaction with the excited intermediate is treated as irreversible and subsequent reaction steps on the bimolecular surface are ignored [3]. Alternative approaches involve coupling two or more master equations [5,7-9]. Recent work by Green and Robertson [10] has presented a generalized pseudo-isomerization methodology for treating any number of such reaction steps in a single master equation in a fully microcanonical manner such that detailed balance is satisfied.

The system studied in the current work involves the HC(O)C(O) radical which is formed as a product in the $\text{OH} + \text{glyoxal}, (\text{CHO})_2$, abstraction reaction (1). The reaction exothermicity for forming $\text{HC(O)C(O)} + \text{H}_2\text{O}$ is $\sim 129 \text{ kJ mol}^{-1}$ [11] and the HC(O)C(O) can then undergo either unimolecular decomposition to form $\text{HCO} + \text{CO}$, reaction (2), or be intercepted by molecular oxygen to form an RO_2 species, HC(O)C(O)O_2 , reaction (3), and then potentially an OH radical via an internal abstraction (reaction (4)) followed by dissociation (reaction (5)) analogous to RO_2/OOH systems in combustion chemistry. [12,13]



54 Glyoxal is an important trace species in the Earth's troposphere and is thought to play a
55 large role in the formation of secondary organic aerosols [14,15]. Both the photochemistry of
56 $(\text{CHO})_2$ and its reaction with OH have been widely studied as these processes predominantly
57 determine its atmospheric lifetime [16-20]. The chemistry of the $\text{HC}(\text{O})\text{C}(\text{O})$ radical formed from
58 reaction (1) was first considered in two chamber studies, [21,22] and theoretical work by da Silva
59 [23] subsequently proposed a mechanism for OH recycling in the $\text{OH} + (\text{CHO})_2$ reaction upon
60 addition of O_2 .

61 Recent work by Lockhart et al. [24] presented an extensive dataset of OH yields as a
62 function of oxygen fraction and total pressure. These OH yield data were obtained by comparing
63 the rate coefficients for OH loss with glyoxal in the presence and absence of oxygen at a particular
64 temperature and total pressure (either pure N_2 or an N_2/O_2 mix). Regeneration of OH from reaction
65 (5) lowers the observed rate coefficient for OH loss in the presence of oxygen allowing for the
66 calculation of the OH yield [24]. However these results are yet to be successfully modelled, with
67 the initial modelling [24] suggesting that non-thermal distributions of the $\text{HC}(\text{O})\text{C}(\text{O})$ radical
68 produced in R1 may be important, raising interesting questions as to the amount of energy
69 partitioned into the spectator component of an abstraction reaction.

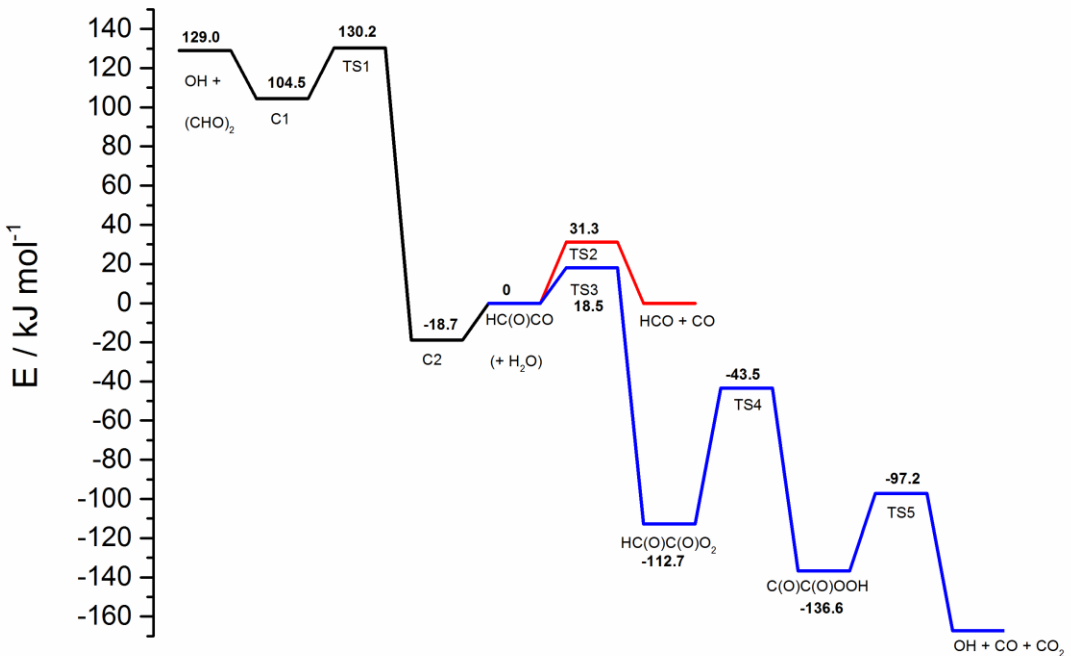
70 There are two extreme models of how energy is partitioned following an abstraction
71 reaction. For a reaction with an early barrier, the reaction exothermicity is expected to be channeled
72 preferentially into the newly formed bond (H_2O for Reaction (1)), leaving little energy in the
73 $\text{HC}(\text{O})\text{C}(\text{O})$ fragment and consequently little dissociation of $\text{HC}(\text{O})\text{C}(\text{O})$. This scenario can lead
74 to high yields of OH via Reactions (3-5). Alternatively, if the reaction exothermicity is distributed
75 statistically, the higher ro-vibrational density of states in the $\text{HC}(\text{O})\text{C}(\text{O})$ fragment will ensure
76 most of the reaction exothermicity is channeled to this fragment, which then rapidly decomposes

77 with consequently no OH formation. This study will explore how the advances in master equation
78 methodology associated with treatment of bimolecular reactions of activated species affect master
79 equation calculations upon the HC(O)C(O) + O₂ system.

80

81 **Theoretical Methodology**

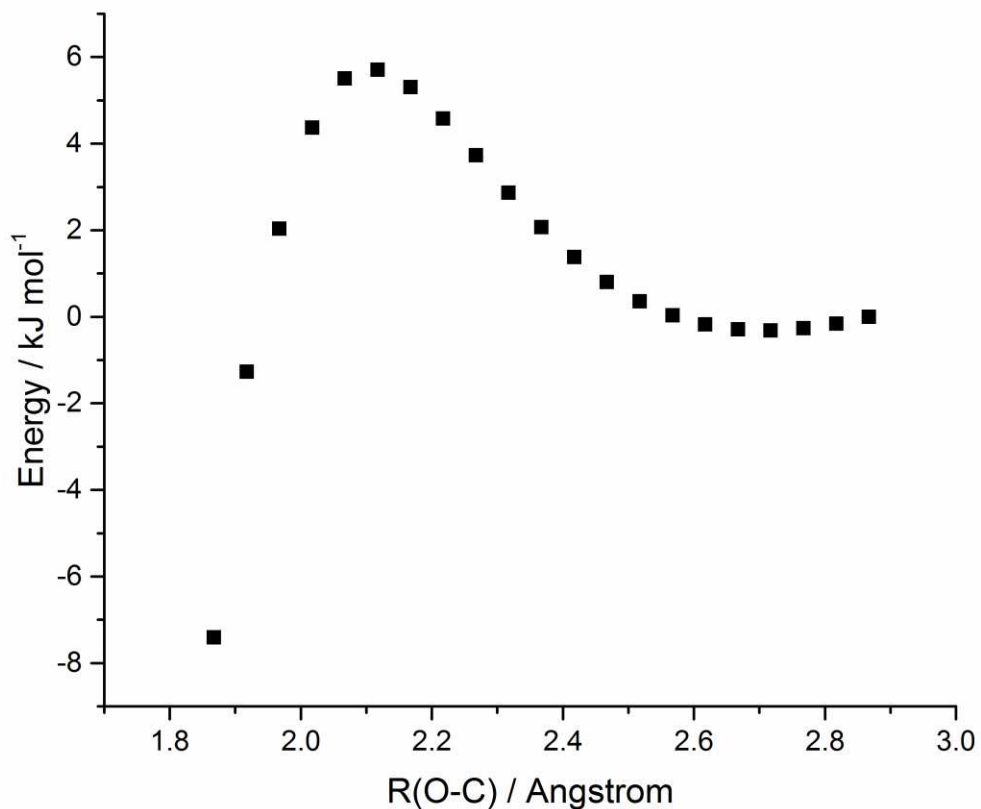
82 The stationary points on the potential energy surface (PES) for the both the HC(O)C(O) + O₂
83 reaction and the unimolecular decomposition of HC(O)C(O) have been characterized previously
84 by da Silva using G3SX model chemistry [23]. In this work the stationary points have been re-
85 characterized with geometry optimizations using the M06-2x/6-311+G(3df,2pd) functional as
86 implemented in the Gaussian 09 [25] suite of programs followed by single point energy
87 calculations at the ROHF-UCCSD(T)-f12b/aug-cc-pVTZ level of theory using Molpro [26].
88 Where appropriate, hindrance potentials for any torsional modes were calculated at the M06-2x/6-
89 31+G(3d,2p) level of theory, through performing constrained geometry optimizations at fixed
90 values of the corresponding dihedral angle. The PES obtained is shown in Figure 1 and is broadly
91 consistent with the calculations of da Silva, [23]. Selected structures are also given in the online
92 supplementary information along with an example MESMER input file including all ro-vibrational
93 information.



94
95 **Figure 1.** Stationary points on the OH + glyoxal + O₂ potential energy surface characterized at the
96 CCSD(T)-f12/aug-cc-pVTZ//MO62x/6-311+G(3df,2pd) level of theory. C1 and C2 denote the pre
97 and post-reaction hydrogen bonded complexes between OH and glyoxal. It is noted that there is a
98 large uncertainty regarding the energy of TS3 (indeed whether it exists at all) and it is highly
99 dependent on the level of theory used.

100
101 As with the work of da Silva, we find in this work that single reference levels of theory
102 predict a saddle point (TS3) on the association path between the HC(O)C(O) radical and O₂,
103 however this region of the PES is strongly multi-configurational in nature and the saddle point
104 could well be an artifact of using a single rather than multi-reference level of theory. The M06-2x
105 method predicts a barrier height of 18.5 kJ mol⁻¹ which seems unreasonably large and CCSD(T)
106 single point calculations at this geometry fail to converge, both issues suggesting significant multi
107 reference effects. The barrier found by da Silva is lower at 1.25 kJ mol⁻¹ [23]. Typically R+O₂

108 reactions are found to be barrierless when multi-reference calculations are used along with a
109 sufficiently large basis set [27,28], however, rs2/ aug-cc-pVTZ calculations with a 5 electron, 7
110 orbital active space consisting of the radical center and the oxygen Π orbitals, do find a transition
111 state. This could arise from either an insufficiently large basis set or other limitations in either the
112 level of theory or the size of the active space. Figure 2 shows a rigid scan along the O-C bond
113 demonstrating the barrier supporting the notion of a transition state to complex formation.



114

115 **Figure 2.** Rigid scan along the O-C bond length in the association between HC(O)C(O) and O₂
116 from rs2/ aug-cc-pVTZ (5o,7e) calculations.

117

118 For the present work we have treated the association step (reaction (3)) using the inverse
 119 Laplace transform (ILT) method [29]. In this method, microcanonical rate coefficients are obtained
 120 by taking the ILT of canonical rate coefficients, k_a , described by the modified Arrhenius form:

$$k_a(T) = A \left(\frac{T}{T_0} \right)^n \exp(-E_a/kT) \quad (6)$$

121 Master equation (ME) calculations were performed using the open source MESMER 4.1 code.[1]
 122 The general formulation of the master equation used in MESMER has been described in detail in
 123 several previous publications [12,27,30] and will not be discussed here.

124 An approach to treating the OH + (CHO)₂ portion of the PES (black PES in Figure 1), is
 125 to include in the ME only that part of the PES from HC(O)C(O) radical onwards and to initialize
 126 the HC(O)C(O) with a prior distribution of energies from the (CHO)₂ + OH reaction. Here the
 127 probability the HC(O)C(O) product is formed with energy E , $P(E)$ is given by [31]:

$$P(E) = \frac{\rho(E)[\rho_t \otimes \rho_{co}](E_x - E)}{[\rho \otimes \rho_t \otimes \rho_{co}](E_x)} \quad (7)$$

128 where E_x exothermicity of the (CHO)₂ + OH reaction, ρ is the ro-vibrational density of states of
 129 HC(O)C(O), ρ_t is the relative translational density of states of the HC(O)C(O) and H₂O fragments
 130 and is modelled using a classical expression i.e. $\rho_t \propto \sqrt{E_t}$ where E_t is the relative translational
 131 energy, ρ_{co} is the ro-vibrational density of states of the H₂O co-product and \otimes represents a
 132 convolution (i.e. $[f \otimes g](E) = \int_0^E f(E-x)g(x)dx$). This approach was not pursued here, partly
 133 because it was desirable to use the whole PES (i.e. including all stationary points to the left of
 134 HC(O)C(O) in Figure 1.), but mostly because Eq. (7) is a poor approximation to the time dependent
 135 energy distribution of the HC(O)C(O) fragment.

136 Using the new pseudo-isomerization methodology, the extended reaction system can be
137 modelled, starting from OH + glyoxal as shown in Figure 1. There are two pseudo-isomerisation
138 steps: the reversible reaction between HC(O)C(O) and H₂O to form the post reaction complex C2
139 and the reversible reaction between HC(O)C(O) and O₂ to form HC(O)C(O)O₂ (R3). For a pseudo
140 isomerization, the dissociation flux, governed by $k(E_i)$ from a grain i in the RO₂ or C2, is
141 partitioned to all grains j of HC(O)C(O) with energy $E_j \leq E_i$ according to a distribution
142 $Q(E_j|E_i)$ of energy E_j being deposited in the HC(O)C(O) fragment. Association rate coefficients
143 can then be obtained through detailed balance. [10]

144 The ME model, initially, included all wells depicted in Figure 1, a grain size of 100 cm⁻¹
145 was used in all calculations and, based on the inspection of eigenvalue span from initial
146 calculations, double-double precision was required for temperatures 295 and 250 K, and quad-
147 double precision was required for temperatures 212 K. Collision parameters used for N₂, the bath
148 gas used in the experiments, were $\varepsilon = 82.0$ K and $\sigma = 3.74$ Å and the collisional energy transfer
149 was treated using an exponential down model [32]. The corresponding parameters for HC(O)C(O)
150 were $\varepsilon = 216$ K and $\sigma = 4.6$ Å based on analogies with glyoxal. Variations in the collision
151 parameters for HC(O)C(O) made little difference to the quality of the fits. (It could be argued that
152 the collision parameters and energy transfer model should be altered as the mole fraction of oxygen
153 is altered, however the error introduced by fixing these parameters is small compared to the other
154 approximations made.) As the temperature range of the experiments was narrow, only temperature
155 independent collision parameters were specified in order to keep the number of variable parameters
156 to a reasonable number. Thus identical values of $\langle \Delta E \rangle_{\text{down}}$ were used for all species, except that of
157 the HC(O)C(O) for which the energy transfer parameter was varied, along with other parameters
158 described below, in order to fit the experimental data. Ro-vibrational densities of states were

159 obtained using a rigid rotor harmonic oscillator approximation with the exception of the torsional
 160 modes which were treated as hindered internal rotations. Any torsional modes were projected from
 161 the molecular Hessian using the method of Sharma et al. [33]. The energy transfer and other
 162 parameters (discussed in the results section) were fit to 88 experimental OH yield data points at
 163 295 K, 250 K and 212 K using a built in Levenburg Marquardt algorithm within MESMER. In
 164 the fitting calculations the following merit function was used:

$$\chi^2(\boldsymbol{\alpha}) = \sum_i \frac{(y_i - y(T_i, p_i, [O_2]_i; \boldsymbol{\alpha}))^2}{\sigma_i^2} \quad (8)$$

165 where y_i are the measured OH yields, $y(T_i, p_i, [O_2]_i; \boldsymbol{\alpha})$ are the calculated yields obtained from
 166 the ME, the vector $\boldsymbol{\alpha}$ being the set of floated parameters and σ_i^2 are the experimental errors.

167 Before fitting the master equation calculations to the experimental data, some initial
 168 simulations were executed. These initial simulations assumed that the $Q(E_j|E_i)$ distribution was
 169 of prior form similar to that in Eq. (7) and as discussed by Green and Robertson [10]:

$$Q(E_j|E_i) = \frac{\rho(E_j)[\rho_t \otimes \rho_{Co}](E_i - E_x - E_j)}{[\rho \otimes \rho_t \otimes \rho_{Co}](E_i - E_x)} \quad (9)$$

170 where the terms are as they were above, but now ρ_{Co} refers to the ro-vibrational density of states
 171 of either H₂O or O₂ depending on the reaction. These simulations demonstrated that the average
 172 amount of energy deposited into the nascent HC(O)C(O) fragment was such that it almost
 173 instantaneously dissociated (reaction 2) leaving no opportunity for reaction with O₂ regardless of
 174 the concentration of oxygen and in contrast to the experimental observations. This is, of course,
 175 hardly surprising given the assumption implied in the use of Eq. (9) that there is complete
 176 microcanonical energy redistribution during the course of a reactive collision between (CHO)₂ and

177 OH; the very large exothermicity combined with instantaneous redistribution means that virtually
178 all HC(O)C(O) fragments would emerge from reaction with energies well in excess of that needed
179 for immediate dissociation.

180 It is clear that a significant reduction in the energy distributed to HC(O)C(O) from that
181 calculated by statistically partitioning the full reaction exothermicity via the prior distribution is
182 required in order to match the experimental data, i.e. the distribution of energy from reaction (1)
183 is far from statistical, but neither does this reaction exhibit an early-barrier, dynamical limit where
184 a majority of the reaction exothermicity is channelled into H₂O vibration [34]. One approach to
185 address this issue is to treat the exothermicity of reaction R1, E_x of Eq. (9), as a parameter to vary.
186 Calculations using the 250 K data were performed and Fig. S1 shows the variation in the yield of
187 OH at high [O₂] as the exothermicity of reaction (1) is varied (i.e. as the prior energy distribution
188 of the HC(O)C(O) is altered). The best fit is obtained when E_x was reduced to 47.2 kJ mol⁻¹, which
189 gave the correct high [O₂] limiting OH yield at 250 K. Clearly, this is significantly different from
190 the 129.0 kJ mol⁻¹ value from the *ab initio* calculations. Whilst good agreement is obtained with
191 experiment with this approach, illustrating that a significant fraction of exothermicity needs to be
192 channeled into the HC(O)C(O) fragment, there is no *a priori* method of estimating the
193 exothermicity required to give good agreement with experiment and therefore this model was not
194 pursued further.

195 Post reaction energy distributions are inherently dynamical processes and this can mean
196 that far more energy is deposited in the newly formed OH bond and therefore in the H₂O molecule
197 than would be predicted statistically by Eq. (9) [34]. For example, a study on a prototypical
198 abstraction reaction:



200 shows considerable excitation in the HF moiety but that the OH is formed cold consistent with a
201 role as a spectator group [35]. Ideally, the way to treat this theoretically for this reaction is to
202 perform classical trajectory calculations as undertaken by Setokuchi [11]. However for this work,
203 the nascent energy distribution $Q(E_j|E_i)$ (Eq. (9)) was modified, so that less energy would go into
204 the internal models of HC(O)C(O) , by the introduction of a new parameter $0 < m \leq 1$, which is
205 used as a power to be applied to the density of states of HC(O)C(O) giving:

$$Q(E_j|E_i) = \frac{(\rho(E_j))^m [\rho_t \otimes \rho_{Co}] (E_i - E_x - E_j)}{[(\rho)^m \otimes \rho_t \otimes \rho_{Co}] (E_i - E_x)} \quad (11)$$

206 This change alters, in an approximate way, the amount of phase space available within the
207 HC(O)C(O) internal modes in which to re-distribute the reaction exothermicity, hence more of this
208 energy appears in the receding H_2O molecule. This model is therefore consistent with the trajectory
209 calculations of Setokuchi which show a significant fraction (53%) of the exothermicity is
210 partitioned to the internal modes of the water product.

211

212 **Results**

213 Initially the three experimental temperature sets were fit individually. In each case the fitted
214 parameters were $\langle \Delta E \rangle_{\text{down}}$, $k_{3\infty}$ (i.e. approximately temperature independent) and the m parameter
215 from Eq. (11). The results of these individual fits are presented in the SI. Inspection of these results
216 show that, while $k_{3\infty}$ was assumed to be approximately independent of temperature, it in fact
217 increases with temperature (albeit not very strongly), that the m parameter appears to have only a

218 weak temperature dependence and that there is significant uncertainty regarding the value
219 of $\langle \Delta E \rangle_{\text{down}}$.

220 The positive temperature dependence of $k_{3\infty}$ suggests a small activation barrier and
221 electronic structure theory calculations, though inconclusive, support this. Related systems would
222 suggest that the presence of a true enthalpy barrier corresponding to TS3 is unlikely. It is also
223 noted that the fitted parameters $k_{3\infty}$ and $\langle \Delta E \rangle_{\text{down}}$ are highly correlated. As such it is unclear how
224 much significance should be placed on the apparent temperature dependence of $k_{3\infty}$. These initial
225 fits were done on the entire PES (i.e. all stationary points were included in the ME model). The portion
226 of the PES for the reaction $\text{HC(O)C(O)} + \text{O}_2 \rightarrow \text{HC(O)C(O)O}_2^* \rightarrow \text{OH} + \text{CO} + \text{CO}_2$, has
227 submerged barriers (TS4 and TS5) with respect to TS3. In a separate set of calculations the effect
228 of increasing the height of TS4 and altering the reversibility of the TS4 reaction was explored at
229 298 K and 5 Torr pressure. Figure 3a shows how the OH yield varies as a fraction of O_2 , f_{O_2} , with
230 different barriers for TS4. As f_{O_2} tends to zero, the oxygen molecule will predominantly collide
231 with a thermalized HC(O)C(O) , whereas as f_{O_2} tends to unity, collisions will be with the chemically
232 activated distribution of HC(O)C(O) and as can be seen there are significant influences on the
233 yield. Also, as the barrier increases, the absolute yield of OH decreases. In Figure 3b, the OH
234 yields have been normalized to the value at $f_{\text{O}_2}=1$ to illustrate that there is change in the shape of
235 the fall-off curve as well as the absolute OH yield. However, with the barrier for TS4 set at the
236 value calculated by the ab initio calculations (-43.5 kJ mol⁻¹ compared to HC(O)C(O)+O_2) an
237 irreversible and reversible treatment of reaction (3) give essentially the same result, and this
238 observation was exploited in subsequent calculations.

239

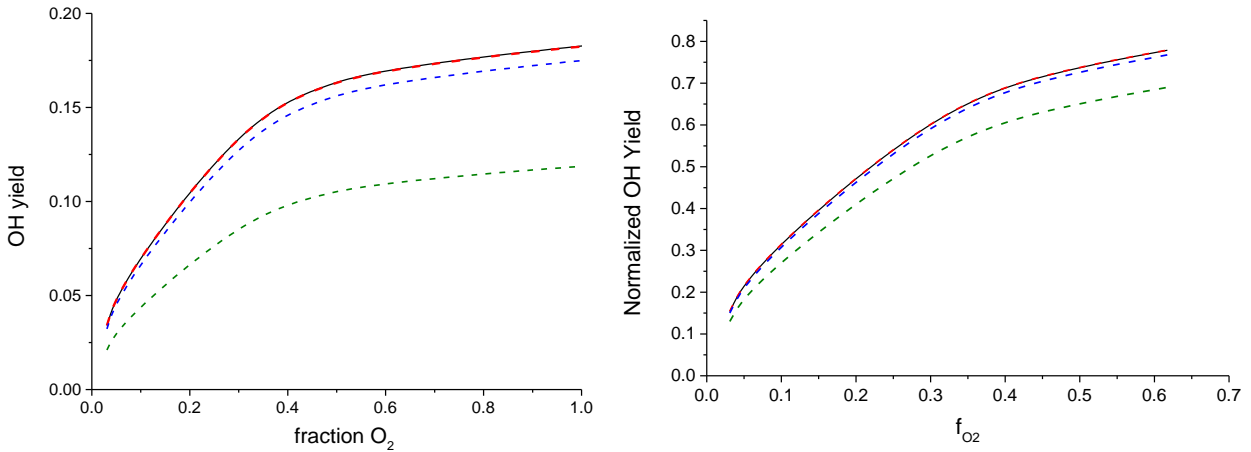


Figure 3a. Variation in the absolute OH yield as a function of fraction of O₂ at various different barrier heights for TS4 (the HCOC(O)O₂ → COC(O)OOH isomerization). Solid black line – reversible treatment, dashed lines – irreversible treatments with barriers -43.5 (red), -26.7 (blue) and -18.3 kJ mol⁻¹ (green) compared to HC(O)C(O) + O₂.

Figure 3b. Variation in the dependence of the normalized OH yield as a function of the fraction of O₂ at various different barrier heights for TS4 at 5 Torr of total pressure. Solid black line – reversible treatment, dashed lines – irreversible treatments with barriers -43.5 (red), -26.7 (blue) and -18.3 kJ mol⁻¹ (green) compared to HC(O)C(O) + O₂.

240 From these observations a combined fitting using all data at once was executed with the
 241 following constraints: the m parameter was taken to be an average over all of the values in the
 242 initial fits and held fixed at 0.256. The ill defined $\langle \Delta E \rangle_{\text{down}}$ parameter was allowed to float but
 243 constrained to be below 400 cm⁻¹, based on a comparison with similar systems.[36,37] k_3 was
 244 constrained to a simple Arrhenius form in order to assess if it was an activated process. To increase
 245 the speed of the calculation the PES was truncated (i.e. made irreversible) after HC(O)C(O)O₂
 246 onwards, the OH yield being equated with the C(O)C(O)OOH yield, this significantly reduced the
 247 size of the ME matrix hence increasing calculation turnaround. The best fit values from the fit are
 248 given in Table 1 along with the 1σ uncertainties. The χ^2 goodness of fit statistic for the fit was
 249 0.00191.

250

251 **Table 1.** Best fit parameters from a fit of data from all temperatures

Parameter	Value	σ
$\langle \Delta E \rangle_{\text{down}} / \text{cm}^{-1}$	388	456
$A_3 / 10^{12} \text{ cm}^3 \text{ molecule}^{-1} \text{ s}^{-1}$	1.69	2.67
$E_3 / \text{kJ mol}^{-1}$	2.41	1.80

252

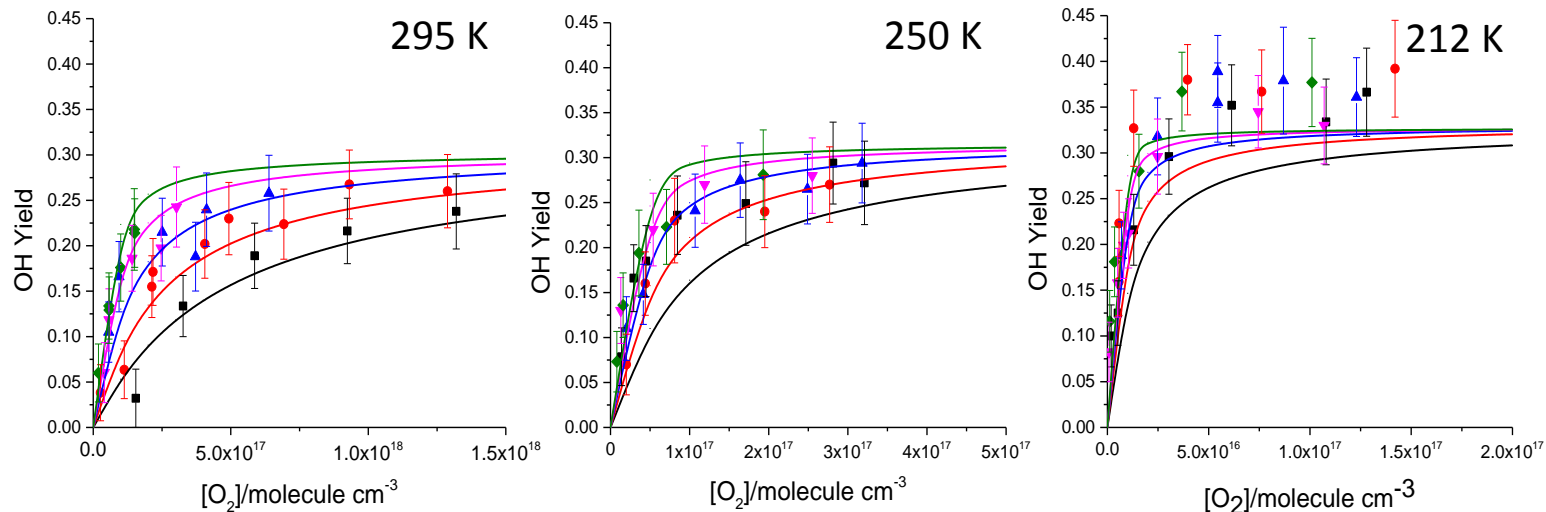
253 Figure 4 show fits to the experimental data at 212, 250 and 295 K. There is a clear
 254 difference in the experimental data between these temperatures which is reproduced by the model.
 255 In all cases, the yield depends on oxygen concentration and tends towards a limiting value as $[O_2]$
 256 increases. At low concentrations of oxygen, HC(O)C(O) decomposition (formally direct or from
 257 HC(O)C(O) initially formed below the dissociation barrier) dominates, but as $[O_2]$ increases
 258 reaction (3) competes more effectively for HC(O)C(O) and the OH yield rises. However, all the
 259 data show that there is a considerable fraction of HC(O)C(O) that is not stabilized associated with
 260 HC(O)C(O) formed from reaction (1) at energies above the dissociation barrier to $\text{HCO} + \text{CO}$. The
 261 fraction of decomposition at high $[O_2]$ ($1 - \Phi_{\text{OH}}$) increases from ~60% at 212 K to ~70% at 295 K,
 262 with the experimental data being qualitatively matched by the model.

263 Pressure dependence in the OH yield, Φ_{OH} , can arise from pressure dependence in either
 264 the HC(O)C(O) dissociation reaction (R2) or the $\text{HC(O)C(O)} + \text{O}_2$ association reaction (R3).
 265 However, the exothermicity and PES of reaction 3, makes this an effectively irreversible process.
 266 At 212 K, there is no obvious pressure dependence in the experimental OH yield, consistent with

267 the HC(O)C(O) dissociation reaction being at its high pressure limit. Conversely at 295 K, there
268 is a significant pressure dependence in Φ_{OH} at a fixed $[\text{O}_2]$ as R2 is in the fall-off region and
269 increasing the total pressure enhances k_2 , increasing the fraction of HC(O)C(O) decomposing.
270 Note also that at 295 K, a significantly higher $[\text{O}_2]$ needs to be added in order for Φ_{OH} to reach half
271 its limiting (i.e. when the rate of non-formally-direct decomposition = rate of reaction 3), as the
272 absolute value of k_2 has a strong positive temperature dependence, whereas that for reaction 3 is
273 either temperature independent or only weakly temperature dependent.

274 The MESMER modeling reproduces the above effects; when the data at various
275 temperatures are fitted individually (see supplementary information), it is possible to better
276 reproduce the changes in the high $[\text{O}_2]$ yields, but only by varying m , i.e. by allowing the fraction
277 of energy channeled into HC(O)C(O) to vary. The value of m at 212 K, 0.233, is significantly
278 lower (i.e. less prompt HC(O)C(O) dissociation) than the value for either 250 or 295 K (0.269 or
279 0.267 respectively). It is not obvious why m should vary with temperature and our discussion
280 focuses mostly on the fitting where m is constant across the three temperatures. In this scenario,
281 the high $[\text{O}_2]$ yields and their slight variation with temperature, fitted the higher temperatures
282 reasonably well, but underestimated the significant jump in the OH yield as the temperature
283 decreased to 212 K. There is also a significant decrease in the modeled pressure dependence of the
284 OH yields as temperature decreases, but there is still a slight overestimation of the pressure
285 dependence at the lower temperatures.

286



287

288 **Figure 4.** Fits to the Experimental Data at 295, 250 and 212 K. (■) 80 Torr, (●) 40 Torr, (▲) 20 Torr, (▼) 10 Torr, (◆) 5 Torr.

289

290 For the experimental data at 295 K, it is possible to estimate the concentration of O₂ at each
 291 pressure at which the OH yield is half the asymptotic yield. At this point the rate of reactions 2
 292 and 3 should be equal. If k_3 is pressure independent ($k_{3,295\text{ K}} = 6.3 \times 10^{-13} \text{ cm}^3 \text{ molecule}^{-1} \text{ s}^{-1}$ from
 293 Table 1), then a value for k_2 can be estimated. Figure 5a shows a plot of k_2 vs [M] and the curvature
 294 of the plot is in the opposite direction from the classic Lindemann plot, i.e. at low total pressures
 295 it is expected that k_2 will vary linearly with pressure, however the values of k_2 appear to lie on a
 296 convex curve, such that the low pressure points are above any straight line that might be inferred
 297 from the high pressure points. This is consistent with HC(O)C(O) molecules formed below the
 298 barrier for dissociation, but still with significant internal energy, playing a role in dissociation. As
 299 pressure is increased (or time for a fixed pressure), these chemically activated molecules become
 300 more thermalized before reaction with O₂ or dissociation. Figure 5b shows the internal energy
 301 distributions of HC(O)C(O) at various times (i.e. with more bath gas collisions) and the clear
 302 relaxation to more thermal distributions is evident.

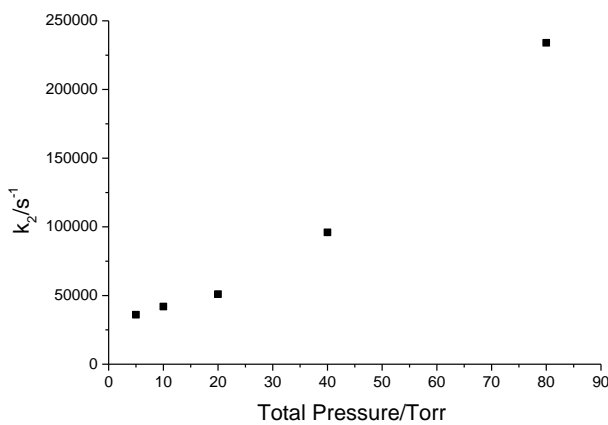


Figure 5a. A plot of k_2 vs pressure showing the pronounced upward curvature at low pressures.

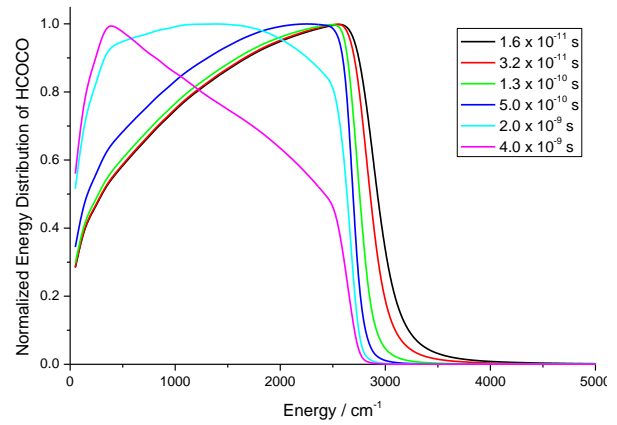


Figure 5b. Thermalization of the HCOCO internal energy (cm⁻¹) distribution with time (s). Conditions are 80 Torr total pressure, 295

K and $[O_2] = 1 \times 10^{18}$ molecule cm⁻³. The reaction threshold is at 2616 cm⁻¹.

303

304 **Conclusions**

305 In this work, the recently developed pseudo isomerization approach is applied for the first time in
306 order to model recent experimental data for the OH + glyoxal + O₂ system. It is demonstrated that
307 this method can be used to extend master equation calculations to include, in theory, any number
308 of non-thermal bi-molecular reactions and despite the complexity of the extended PES used in the
309 current work, the master equation results can be fit to the experimental data. Using this approach
310 the [O₂] dependence of the observed OH yields for this system have been reproduced theoretically
311 for the first time although there are still discrepancies between experiment and theory, particularly
312 at low temperatures. It is clear from the errors reported in Table 1 that only a limited amount of
313 information can be extracted from the data.

314 This work also highlights the differences between a full model using a pseudo
315 isomerization method, and more approximate approaches. In particular it is noted that including
316 the OH + glyoxal portion of the PES captures the temperature dependence of the prompt
317 HC(O)C(O) decomposition which a model using HC(O)C(O) initialized with a prior distribution
318 cannot do. The temperature dependence observed with the full model includes a thermal
319 component to the initial HC(O)C(O) energy.

320 There remain two particular areas of uncertainty in the glyoxal + OH + O₂ system, which
321 warrant further investigation: firstly, the value of the m parameter, which was fixed at 0.256 during
322 the main fitting, suggests that effective density of states of the HC(O)C(O) fragment, is
323 considerably less than the might be expected on simple statistical grounds, and further suggests

324 that not all glyoxal molecular degrees of freedom participate in the R1. Some speculative
325 rationalization can be drawn from considering the degrees of freedom of the HC(O)C(O): an
326 approximate classical model of 9 vibrational modes, 3 rotational modes and 3 translational modes
327 would yield a density of states $\rho(E_j) \propto E^{11}$ if however all the vibrational modes are assumed not
328 to contribute, the effective density of states would be $\rho(E_j) \propto E^2$ giving a value of m of 0.182. The
329 discrepancy between the values of 0.182 and 0.256 suggests that there is either some vibrational
330 contribution or perhaps that the rotations cannot be treated as free. While this speculation might
331 seem reasonable, given the short length of time of a reactive collision, it remains difficult to predict
332 a priori what the value of m should be, and it is clear that detailed dynamical calculations are
333 required in order investigate the general form of the product energy distribution ($Q(E_j|E_i)$ of Eq.
334 (11)) of HC(O)C(O) emerging from R1. For the purposes of this work, it suffices to acknowledge
335 the additional level of detail that can be obtained by treating extended mechanisms fully reversibly
336 in a single master equation, since such thermal effects would be missed if the HC(O)C(O) were
337 simply initialized with a prior distribution of energies.

338 The other main source of uncertainty surrounds the HC(O)C(O) + O₂ process. Comparison
339 with similar systems would suggest that this process is barrierless and it is likely that the barrier
340 observed in electronic structure theory calculations is an artifact due to limitations in the level of
341 theory used. However the ILT results show that this reaction has a low A factor of 1.69×10^{-12}
342 molecule⁻¹ cm³ s⁻¹, and while such a low value is not completely unprecedented, [38] this process
343 certainly warrants more detailed consideration in the form of multi-faceted, variational
344 calculations of the association rate coefficient.

345 **Supporting Information.** An example MESMER input file including all energetic and ro-
346 vibrational data for the current system is available in the supporting information. In addition the
347 supporting information shows the structures of each stationary point on the PES. This material is
348 available free of charge via the Internet at doi.....

349 **Corresponding Authors**

350 *Emails: p.w.seakins@leeds.ac.uk, struanhrobertson@gmail.com .

351 **Notes**

352 The authors declare no competing financial interests.

353

354 **ACKNOWLEDGMENT**

355 Support for RJS, MAB and PWS from EPSRC Grant EP/J01871/1 is gratefully acknowledged.

356

357 **REFERENCES**

358

- 359 [1] D.R. Glowacki, C.H. Liang, C. Morley, M.J. Pilling, S.H. Robertson, J. Phys. Chem. A 116 (2012)
360 9545.
- 361 [2] T.J. Frankcombe, S.C. Smith, K.E. Gates, S.H. Robertson, Phys. Chem. Chem. Phys. 2 (2000) 793.
- 362 [3] D.R. Glowacki, J. Lockhart, M.A. Blitz, S.J. Klippenstein, M.J. Pilling, S.H. Robertson, P.W. Seakins,
363 Science (Washington, D. C., 1883-) 337 (2012) 1066.
- 364 [4] J. Lockhart, M.A. Blitz, D.E. Heard, P.W. Seakins, R.J. Shannon, J. Phys. Chem. A 117 (2013) 5407.
- 365 [5] M.P. Burke, C.F. Goldsmith, Y. Georgievskii, S.J. Klippenstein, Proceedings of the Combustion
366 Institute 35 (2015) 205.
- 367 [6] C.F. Goldsmith, M.P. Burke, Y. Georgievskii, S.J. Klippenstein, Proceedings of the Combustion
368 Institute 35 (2015) 283.
- 369 [7] M. Pfeifle, M. Olzmann, Int. J. Chem. Kinet. 46 (2014) 231.
- 370 [8] G. da Silva, J. Phys. Chem. A 116 (2012) 5317.
- 371 [9] A. Maranzana, J.R. Barker, G. Tonachini, Phys. Chem. Chem. Phys. 9 (2007) 4129.
- 372 [10] N.J.B. Green, S.H. Robertson, Chem. Phys. Lett. 605 (2014) 44.
- 373 [11] O. Setokuchi, Phys. Chem. Chem. Phys. 13 (2011) 6296.
- 374 [12] A.J. Eskola, S.A. Carr, R.J. Shannon, B. Wang, M.A. Blitz, M.J. Pilling, P.W. Seakins, S.H. Robertson,
375 J. Phys. Chem. A 118 (2014) 6773.

- 376 [13] J. Zador, C.A. Taatjes, R.X. Fernandes, Progress in Energy and Combustion Science 37 (2011) 371.
- 377 [14] T.M. Fu, D.J. Jacob, F. Wittrock, J.P. Burrows, M. Vrekoussis, D.K. Henze, Journal of Geophysical
- 378 Research-Atmospheres 113 (2008) 17.
- 379 [15] J. Liggio, S.M. Li, R. McLaren, Journal of Geophysical Research-Atmospheres 110 (2005) 13.
- 380 [16] K.J. Feierabend, J.E. Flad, S.S. Brown, J.B. Burkholder, J. Phys. Chem. A 113 (2009) 7784.
- 381 [17] K.J. Feierabend, L. Zhu, R.K. Talukdar, J.B. Burkholder, J. Phys. Chem. A 112 (2008) 73.
- 382 [18] R.J. Salter, M.A. Blitz, D.E. Heard, T. Kovacs, M.J. Pilling, A.R. Rickard, P.W. Seakins, Phys. Chem.
- 383 Chem. Phys. 15 (2013) 4984.
- 384 [19] R.J. Salter, M.A. Blitz, D.E. Heard, M.J. Pilling, P.W. Seakins, Phys. Chem. Chem. Phys. 15 (2013)
- 385 6516.
- 386 [20] F. Wittrock, A. Richter, H. Oetjen, J.P. Burrows, M. Kanakidou, S. Myriokefalitakis, R. Volkamer, S.
- 387 Beirle, U. Platt, T. Wagner, Geophys. Res. Lett. 33 (2006) L16804.
- 388 [21] H. Niki, P.D. Maker, C.M. Savage, L.P. Breitenbach, Int. J. Chem. Kinet. 17 (1985) 547.
- 389 [22] J.J. Orlando, G.S. Tyndall, Int. J. Chem. Kinet. 33 (2001) 149.
- 390 [23] G. da Silva, Phys. Chem. Chem. Phys. 12 (2010) 6698.
- 391 [24] J. Lockhart, M. Blitz, D. Heard, P. Seakins, R. Shannon, J. Phys. Chem. A 117 (2013) 11027.
- 392 [25] M.J. Frisch, G.W. Trucks, H.B. Schlegel, G.E. Scuseria, M.A. Robb, J.R. Cheeseman, G. Scalmani, V.
- 393 Barone, B. Mennucci, G.A. Petersson, H. Nakatsuji, M. Caricato, X. Li, H.P. Hratchian, A.F.
- 394 Izmaylov, J. Bloino, G. Zheng, J.L. Sonnenberg, M. Hada, M. Ehara, K. Toyota, R. Fukuda, J.
- 395 Hasegawa, M. Ishida, T. Nakajima, Y. Honda, O. Kitao, H. Nakai, T. Vreven, J. Montgomery, J. A.;
- 396 J.E. Peralta, F. Ogliaro, M. Bearpark, J.J. Heyd, E. Brothers, K.N. Kudin, V.N. Staroverov, R.
- 397 Kobayashi, J. Normand, K. Raghavachari, A. Rendell, J.C. Burant, S.S. Iyengar, J. Tomasi, M. Cossi,
- 398 N. Rega, J.M. Millam, M. Klene, J.E. Knox, J.B. Cross, V. Bakken, C. Adamo, J. Jaramillo, R.
- 399 Gomperts, R.E. Stratmann, O. Yazyev, A.J. Austin, R. Cammi, C. Pomelli, J.W. Ochterski, R.L.
- 400 Martin, K. Morokuma, V.G. Zakrzewski, G.A. Voth, P. Salvador, J.J. Dannenberg, S. Dapprich, A.D.
- 401 Daniels, Ö. Farkas, J.B. Foresman, J.V. Ortiz, J. Cioslowski, D.J. Fox, Gaussian 09, Revision **A.1**.
- 402 Gaussian, Inc., Wallingford CT, 2009.
- 403 [26] H.-J. Werner, P.J. Knowles, G. Knizia, F.R. Manby, M. Schütz, P. Celani, T. Korona, R. Lindh, A.
- 404 Mitrushenkov, G. Rauhut, K.R. Shamasundar, T.B. Adler, R.D. Amos, A. Bernhardsson, A. Berning,
- 405 D.L. Cooper, M.J.O. Deegan, A.J. Dobbyn, F. Eckert, E. Goll, C. Hampel, A. Hesselmann, G. Hetzer,
- 406 T. Hrenar, G. Jansen, C. Köppl, Y. Liu, A.W. Lloyd, R.A. Mata, A.J. May, S.J. McNicholas, W. Meyer,
- 407 M.E. Mura, A. Nicklass, D.P. O'Neill, P. Palmieri, D. Peng, K. Pflüger, R. Pitzer, M. Reiher, T.
- 408 Shiozaki, H. Stoll, A.J. Stone, R. Tarroni, T. Thorsteinsson, M. Wang, MOLPRO, version 2012.1, a
- 409 package of *ab initio* programs, 2012.
- 410 [27] S.A. Carr, D.R. Glowacki, C.H. Liang, M.T. Baeza-Romero, M.A. Blitz, M.J. Pilling, P.W. Seakins, J.
- 411 Phys. Chem. A 115 (2011) 1069.
- 412 [28] A.M. Knepp, G. Meloni, L.E. Jusinski, C.A. Taatjes, C. Cavallotti, S.J. Klippenstein, Phys. Chem.
- 413 Chem. Phys. 9 (2007) 4315.
- 414 [29] S.H. Robertson, M.J. Pilling, D.L. Baulch, N.J.B. Green, J. Phys. Chem. 99 (1995) 13452.
- 415 [30] S.A. Carr, T.J. Still, M.A. Blitz, A.J. Eskola, M.J. Pilling, P.W. Seakins, R.J. Shannon, B. Wang, S.H.
- 416 Robertson, J. Phys. Chem. A 117 (2013) 11142.
- 417 [31] M. Baer, W.L. Hase, Unimolecular Reaction Dynamics, Oxford University Press, Oxford, 1986.
- 418 [32] K.A. Holbrook, M.J. Pilling, S.H. Robertson, Unimolecular Reactions, Wiley, Chichester, 1996.
- 419 [33] S. Sharma, S. Raman, W.H. Green, J. Phys. Chem. A 114 (2010) 5689.
- 420 [34] J.C. Polanyi, Science 236 (1987) 680.
- 421 [35] J. Li, R. Dawes, H. Guo, J. Chem. Phys. 137 (2012).
- 422 [36] A.W. Jasper, C.M. Oana, J.A. Miller, Proceedings of the Combustion Institute 35 (2015) 197.
- 423 [37] K. McKee, M.A. Blitz, M.J. Pilling, J. Phys. Chem. A 120 (2016) 1408.

424 [38] J. Zador, H.F. Huang, O. Welz, J. Zetterberg, D.L. Osborn, C.A. Taatjes, *Phys. Chem. Chem. Phys.*
425 15 (2013) 10753.

426

427